Supporting Information

Boriskina and Reinhard 10.1073/pnas.1016181108

SI Text

High-Q optical microcavities can strongly modify the local density of electromagnetic states (LDOS) and thus can be used for the frequency-selective enhancement (suppression) of the radiative rates of emitters either evanescently coupled to or embedded inside the cavities. The enhancement is characterized by the Purcell factor, and can be large in cavities that support optical modes with high quality factors and small mode volumes (1–5). Fig. S1 illustrates this effect for a model structure composed of a single dipole emitter with a transition moment oriented along the y-axis, which is evanescently coupled to a microsphere via a 1nm-wide airgap (Fig. S1*A*). The spectra of the microcavity-mediated dipole radiative rate enhancement shown in Fig. S1*B* feature a series of sharp peaks that correspond to the dipole emission coupling to the whispering-gallery (WG) modes inside the microspheres. The spectral positions of the resonances are determined by the morphology of the microcavity (its size and material composition), and the resonance linewidths are inversely proportional to the WG mode *Q*-factors.

In general, each WG mode in a microsphere can be specified by four indices: n, the radial order (the number of peaks in the intensity profile along the radial direction); m, the azimuthal mode index (the number of field variations along the sphere equator); l, the number of waves in a cyclic orbit ($l - |m| + 1$ is equal to the number of peaks in the intensity profile of the mode along the meridian); and polarization, TE (transverse-electric) or TM (transverse magnetic) (6, 7). Each WG mode is multiple-degenerate in frequency with m taking the values $l, l-1 \ldots -l$ for each n. Our simulations show that the most pronounced spectral peaks in Fig. S1*B* correspond to the excitation of TE-polarized WG modes with $n = 1$ and $m = l$ in the microsphere (see Fig. S2), which are indexed as $TE_{m,1}$ modes in Fig. S1*B*. The spectra of the electric field intensity monitored on the opposite side of the microspheres demonstrate narrow-peak resonant enhancement produced by the evanescent tails of the WG modes (Fig. S1*C*). However, as the optical leakage of the WG modes occurs along the whole circumference of the sphere, light refocusing into a nanoscale volume cannot be achieved. Typical electric field intensity distributions of TE_{nm} modes in microsphere resonators are shown in Fig. S2.

Strong coherent coupling of the fields of nanoscale emitters to surface plasmon resonances in noble-metal nanostructures also results in strong modification of their radiative and nonradiative decay rates (8–10). In this case, the Purcell enhancement of dipole emission is enabled by the strongly reduced effective mode volume for the photons, while the *Q*-factors of plasmonic nanostructures are limited by high dissipative losses in metals at optical wavelengths. A schematic of a nanoantenna-coupled dipole source is shown in Fig. S3*A* together with the second acceptor nanoantenna, which is separated from the donor one by a micron-scale distance L. The spectra of the nanoantenna-mediated emitter radiative rate enhancement feature a single broad peak that corresponds to the excitation of the bonding dipole plasmon resonance of the nanodimer (with the peak wavelength determined by the Au nanoparticles radii and the antenna gap width, see Fig. S3*B*). The spectra of the field intensity measured in the gap of the acceptor nanodimer also feature a single broad peak (Fig. S3*C*). However, a free-space energy transfer between two plasmonic nanoantennas is not efficient as most of the energy radiated by the donor nanoantenna cannot be recaptured by the acceptor antenna (see Fig. 1 *F* and *G*).

The results of our simulations shown in Fig. 1 of the main text demonstrate that a combination of the high *Q*-factors of the microcavity modes and the strong field localization in the gap of plasmonic antennas result in the resonant increase of the dipole radiative rates over the values achievable either by using a microcavity or an antenna alone. In the optoplasmonic superlens configuration considered in this paper, plasmonic antennas interact with the microcavity modes via the exponentially decaying tails of their evanescent fields (Fig. S4*A*). Therefore, the interaction is distance-dependent and, as shown in Fig. S4*B*, the amplitude of the effect reduces with the antenna-cavity separation. However, the data in Fig. S4*B* demonstrate a high tolerance of the values of the radiative rate enhancement to the variations (up to tens of nanometers) in the width of the antenna-cavity gap. Furthermore, our calculations show that coupling of the antenna to the microcavity not only can enhance the dipole radiative rate but also increases its external quantum efficiency (Fig. S4*C*). Finally, the efficiency of the light refocusing in the acceptor antenna is robust to small variations in the antenna-microcavity coupling distance (Fig. S4 *D* and *E*).

As mentioned in the main text, a number of nano-fabrication techniques can be used to fabricate the proposed bright- and dark-field optoplasmonic superlenses and on-chip integrated optoplasmonic networks. Some of the examples of possible realizations of the optoplasmonic components and circuits are shown in Fig. S5 and can include not only spherical particles or microcavities but also planar microdisk, microring and microtoroid resonators as well as bow-tie and other types of dimer gap antennas and metal nanoclusters.

1. Barclay PE, Santori C, Fu K-M, Beausoleil RG, Painter O (2009) Coherent interference effects in a nano-assembled diamond NV center cavity-QED system. *Opt Express* 17:8081–8097.
2. Englund D, et al. (2005) Controlling the spontaneous emission rate of single quantum dots in a two-dimensional photonic crystal. *Phys Rev Lett.* 95:013904.
3. Badolato A, et al. (2005) Deterministic coupling of single quantum dots to single nanocavity modes. *Science* 308:1158–1161.
4. Vernooy DW, Furusawa A, Georgiades NP, Ilchenko VS, Kimble HJ (1998) Cavity QED with high-Q whispering gallery modes. *Phys Rev A* 57:R2293.
5. Armani AM, Vahala KJ (2006) Heavy water detection using ultra-high-Q microcavities. *Opt Lett* 31:1896–1898.
6. Johnson BR (1993) Theory of morphology-dependent resonances: Shape resonances and width formulas. *J Opt Soc Am A* 10:343–352.
7. Teraoka I, Arnold S (2009) Resonance shifts of counterpropagating whispering-gallery modes: Degenerate perturbation theory and application to resonator sensors with axial symmetry. *J Opt Soc Am B* 26:1321–1329.
8. Kühn S, Håkanson U, Rogobete L, Sandoghdar V (2006) Enhancement of single-molecule fluorescence using a gold nanoparticle as an optical nanoantenna. *Phys Rev Lett* 97:017402.
9. Bharadwaj P, Deutsch B, Novotny L (2009) Optical antennas. *Adv Opt Photon* 1:438–483.
10. Chang DE, Sorensen AS, Hemmer PR, Lukin MD (2006) Quantum optics with surface plasmons. *Phys Rev Lett.* 97:053002.
11. Smythe EJ, Dickey MD, Whitesides GM, Capasso F (2008) A technique to transfer metallic nanoscale patterns to small and non-planar surfaces. *ACS Nano* 3:59–65.
12. Barth M, et al. (2010) Nanoassembled plasmonic-photonic hybrid cavity for tailored light-matter coupling. *Nano Lett* 10:891–895.
13. Curto AG, et al. (2010) Unidirectional emission of a quantum dot coupled to a nanoantenna. *Science* 329:930–933.
14. Lipomi DJ, et al. (2010) Fabrication and replication of arrays of single- or multicomponent nanostructures by replica molding and mechanical sectioning. *ACS Nano* 4:4017–4026.

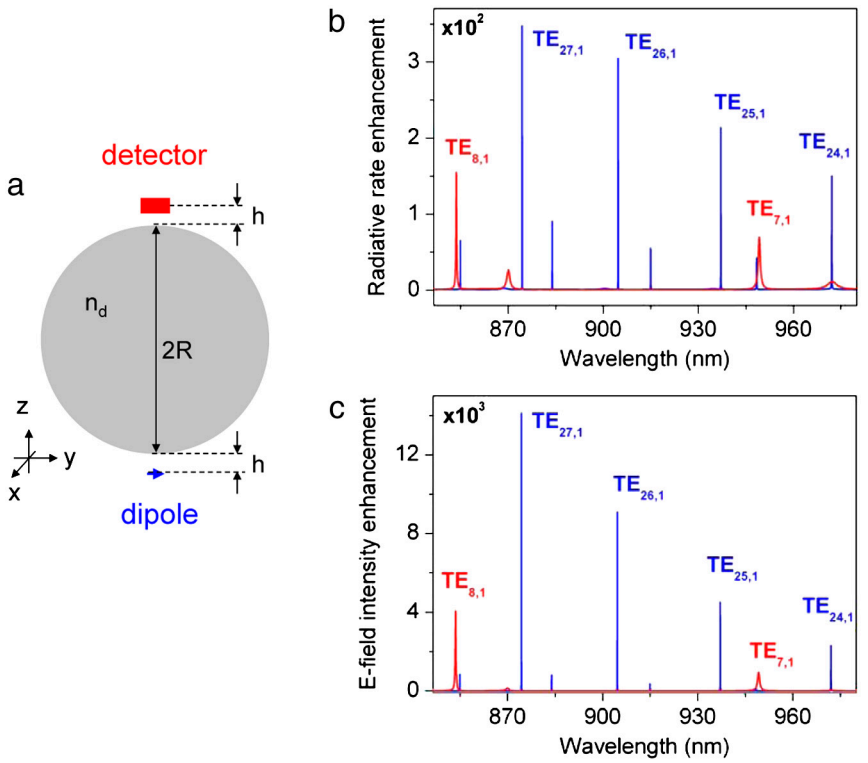

Fig. S1. (*A*) A schematic of the microsphere excited by a dipolar source (blue arrow, $h = 1$ nm) and the position of the detector monitoring the electric field (red bar). (*B*) The dipole radiative rate enhancement (over the free-space value) as a function of wavelength and the sphere morphology (blue: $R = 2.8$ μm, $n_d = 1.59$, $h = 1$ nm; red: $R = 0.65$ μm, $n_d = 2.4$, $h = 1$ nm). The resonant peaks correspond to the excitation of the WG modes in the microspheres. (*C*) Electric field intensity enhancement at the detector position (over the value generated by a free-space dipole at the same position).

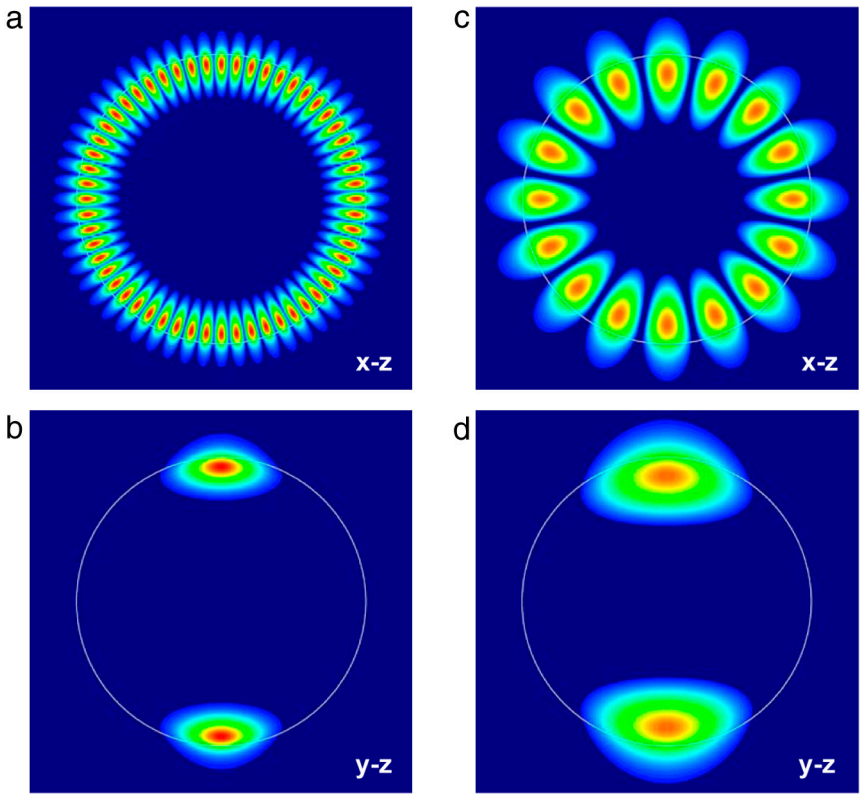

Fig. S2. (*A–D*) Field intensity distributions in the x-z (*A* and *C*) and y-z (*B* and *D*) planes of the $TE_{28,1}$ whispering-gallery mode in a larger polystyrene microsphere (*A*, *B*, $R = 2.8$ μm, $n_d = 1.59$, $\lambda_{res} = 846.12$ nm, $Q = 1.05 \cdot 10^5$) and of the $TE_{8,1}$ WG mode in a smaller TiO_2 microsphere (*C*, *D*, $R = 650$ nm, $n_d = 2.4$, $\lambda_{res} = 853.62$ nm, $Q = 3204$).

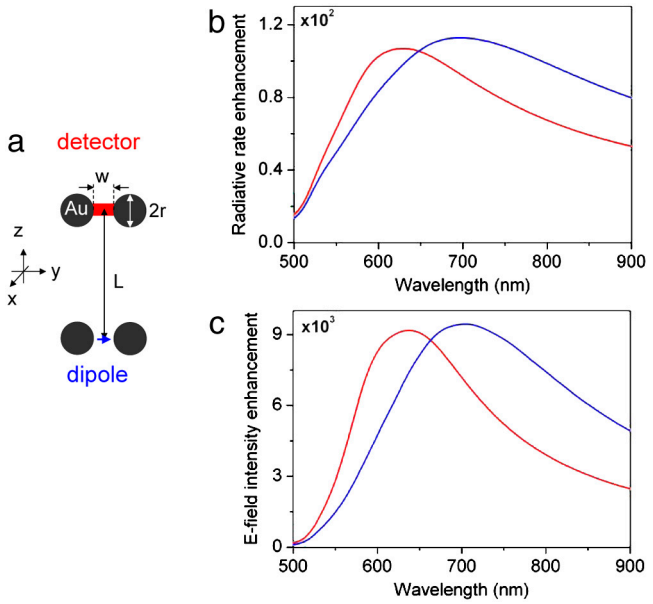

Fig. S3. (*A*) A schematic of two Au nanodimer antennas showing a position of the dipole emitter and the field intensity monitor. (*B*) Radiative rate enhancement (over the free-space value) of the dipole positioned in the gap of the donor antenna as a function of wavelength and antenna geometry (red: $r = 65$ nm, $w = 25$ nm, $L = 652$ nm; blue: $r = 75$ nm, $w = 25$ nm, $L = 2.802$ μm). (*C*) Electric field intensity enhancement in the gap of the acceptor antenna (over the value generated by a free-space dipole at the same position).

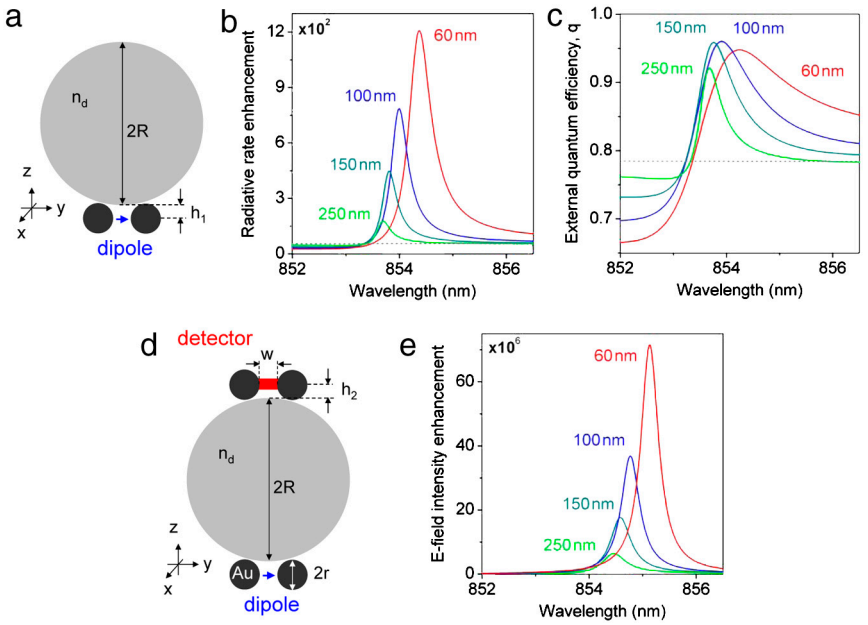

Fig. S4. (*A*) A schematic of an Au nanodimer antenna coupled to a microcavity via an airgap of width h_1 ($R = 650$ nm, $n_d = 2.4$, $r = 55$ nm, $w = 20$ nm) (*B*) Radiative rate enhancement of a dipole positioned in the center of the antenna gap as a function of the wavelength around one of the WG mode peaks and the antenna-microcavity separation h_1. The labels indicate the values of h_1, and the dashed line shows the antenna-mediated dipole radiative rate enhancement in the absence of the microcavity. (*C*) External quantum efficiency q of the antenna-microcavity structure. The dashed line shows the corresponding value of the nanodimer antenna. (*D*) A schematic of the optoplasmonic superlens with the acceptor antenna separated from the microcavity via the airgap of width h_2. (*E*) Electric field intensity enhancement in the gap of the acceptor antenna as a function of wavelength and h_2 ($h_1 = 60$ nm, the labels indicate the values of h_2).

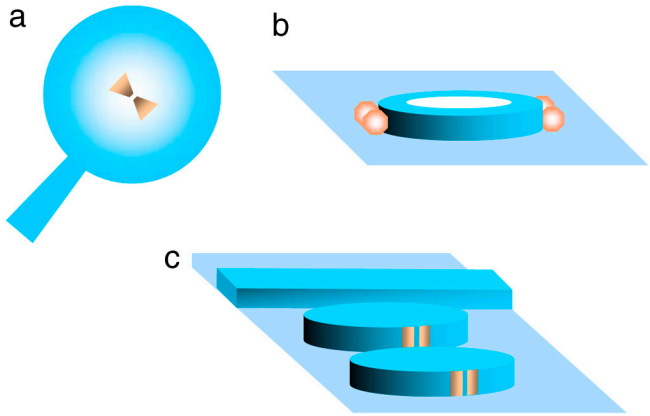

Fig. S5. (*A*) Plasmonic nanoantenna(s) can be transferred to a surface of a dielectric microsphere (11). (*B*) On-chip microdisk or microring resonators decorated with nanosphere dimers can be fabricated by a combination of lithography and nanomanipulation (12). (*C*) Planar networks of dielectric (semiconductor) microdisks laterally coupled to plasmonic nanoantennas and photonic nanowire waveguides are also amenable to fabrication by two-step conventional and soft lithographic techniques (13, 14).